In-situ functionalization of a cellulosic-based activated carbon with magnetic iron oxides for the removal of carbamazepine from wastewater

Diogo Pereira[1], Luciana S. Rocha[1], María V. Gil[2], Marta Otero[3], Nuno J. O. Silva[4], Valdemar I. Esteves[1], Vânia Calisto[1*]

[1]*Department of Chemistry & CESAM, University of Aveiro, Campus de Santiago, 3810-193 Aveiro, Portugal*

[2] *Instituto de Ciencia y Tecnología del Carbono, INCAR-CSIC, Apartado 73, 33080 Oviedo, Spain.*

[3]*Department of Environment and Planning & CESAM, University of Aveiro, Campus de Santiago, 3810-193 Aveiro, Portugal*

[4]*Department of Physics & CICECO, University of Aveiro, Campus de Santiago, 3810-193 Aveiro, Portugal*

**corresponding author: vania.calisto@ua.pt*

Abstract

The main goal of this work was to produce an easily recoverable waste-based magnetic activated carbon (MAC) for an efficient removal of the anti-epileptic pharmaceutical carbamazepine (CBZ) from wastewater. For this purpose, the synthesis procedure was optimized and a material (MAC4) providing immediate recuperation from solution, remarkable adsorptive performance and relevant properties (specific surface area (S_{BET}) of 551 m^2 g^{-1} and saturation magnetization of 39.84 emu g^{-1}) was selected for further CBZ kinetic and equilibrium adsorption studies. MAC4 presented fast CBZ adsorption rates and short equilibrium times (<30-45 min) in both ultrapure water and wastewater. Equilibrium studies showed that MAC4 attained maximum adsorption capacities (q_m) of 68 ± 4 mg g^{-1} in ultrapure water and 60 ± 3 mg g^{-1} in wastewater, suggesting no significant interference of the aqueous matrix in the adsorption process. Overall, this work provides evidence of potential application of a waste-based MAC in the tertiary treatment of wastewaters.

Keywords (8)

Magnetic recuperation, Waste-based magnetic carbon, Paper mill sludge, *In situ* coprecipitation, Wastewater treatment, Emerging contaminants, Micropollutants, Water quality

1. Introduction

Modern human and veterinary health care strongly rely on pharmaceuticals consumption. The European Union (EU) alone accounts for 25% of the global pharmaceutical market and the forecasts point to a continuous growth of consumption (Deloitte Sustainability 2018). These substances are considered the source of tremendous benefits to public health but, in the meantime, are becoming increasingly ubiquitous in several environmental matrices, being detected in the ng to low µg per litre range (Jelic et al. 2012; Pereira et al. 2017; Desbiolles et al. 2018; McCance et al. 2018). Continuous exposure to pharmaceuticals may pose a significant risk to humans and has been proved to have severe disruptive effects in ecosystems (Pomati et al. 2006; Kidd et al. 2007; Malchi et al. 2014; Vasquez et al. 2014; de Jesus Gaffney et al. 2015; Niemuth and Klaper 2015). The EU has recognized the importance of developing measures to regulate this issue (Parliament 2013) and several pharmaceuticals have recently integrated a Union-wide monitoring list that aims to provide relevant data to support future inclusions in the list of priority substances in the field of water policy (European Commission 2015, 2018).

Currently, wastewater treatment plants (WWTP) are incapable of efficiently removing pharmaceuticals (Calisto and Esteves 2009; Rivera-Utrilla et al. 2013; Pereira et al. 2015) being the primary entry pathway of these compounds into the environment (Jelic et al. 2011; Luo et al. 2014). A conventional WWTP operation is based on physicochemical (primary) and biological (secondary) processes, which are designed to eliminate suspended solids, inorganic nutrients and biodegradable organic matter (Nakada et al. 2007). As for hydrophilic and non-biodegradable contaminants, such as pharmaceuticals, an extra step of treatment (tertiary) is required to successfully remove them from the final effluent. For instance, the antiepileptic carbamazepine (CBZ) generally presents WWTP removal efficiencies below 10 % (Zhang et al. 2008; Bahlmann et al. 2014). The incorporation of an advanced tertiary step, functioning as an effluent refinement stage before the release into the environment, is not a common practice in the majority of WWTP. The main obstacle lies with the high costs, the generation of

transformation by-products and the operation complexity associated with tertiary treatments, such as membrane filtration or advanced oxidation processes (Zimmermann et al. 2011).

In the described context, adsorption appears to be a promising alternative for the removal of organic contaminants from water due to its versatility, high removal efficiency in a short time, effectiveness, no undesired by-product formation and the possibility of regeneration/reuse of the exhausted adsorbent (Altmann et al. 2014; Bayramoglu et al. 2016, 2020; Bayramoglu and Arica 2018). Currently, activated carbon is the most commonly used adsorbent in wastewater treatment. However, the production cost of commercial coal-based activated carbon is often considered prohibitive for its large-scale application. As a possible solution, several agricultural and industrial wastes have been successfully applied as activated carbon precursors (Ioannidou and Zabaniotou 2007; Cazetta et al. 2011; Jaria et al. 2017; Satayeva et al. 2018; Oliveira et al. 2018) both lowering production costs and creating a sustainable and innovative waste management strategy (Silva et al. 2018). Powdered activated carbon (PAC) has proved to be highly efficient in the removal of pharmaceuticals (Serrano et al. 2011; Nielsen et al. 2014; Silva et al. 2019), including CBZ (Li et al. 2011; To et al. 2017; Delgado et al. 2019), with several pilot and large-scale studies on effluent wastewater pointing the significant increment in removal efficiency brought to the WWTP and substantiating the viability of a full-scale implementation of this technology (Boehler et al. 2012; Margot et al. 2013; Mailler et al. 2015; Meinel et al. 2016; Kårelid et al. 2017; Guillossou et al. 2019). Nonetheless, a generalized integration of PAC treatment in WWTP systems is still limited, particularly due to its small particle size, which hampers the separation from the treated effluent. Typically, the recuperation of the exhausted PAC is achieved by flocculation/coagulation, sedimentation, filtration (sand or membranes), or a combination of these processes, which tend to be costly, time consuming and impede the PAC recuperation. As a promising alternative, magnetic activated carbon (MAC) combines the adsorption performance of PAC with immediate magnetic retrievability. Magnetic response is achieved through functionalization of PAC surface with magnetic nanoparticles, the magnetic

iron oxides magnetite and maghemite being the most typically employed because of their availability and simplicity of preparation (Luiz, Oliveira et al. 2002; Hao et al. 2018). Coating the surface of PAC with magnetic nanoparticles allows its recuperation from the treated effluent through the application of an external magnetic field gradient. As of recently, MAC has been successfully employed in the adsorption of several pharmaceuticals from water. Some examples include the works of Baghadadi et al. (2016) in the removal of CBZ from real wastewater using a magnetized commercial PAC; or Wong et al. (2016) applying a commercial waste-based phenyl-functionalized magnetic PAC in the removal of CBZ from water, among other pharmaceuticals. However, most of these studies involved the magnetization of commercial PAC and very few include adsorption experiments using WWTP effluents (Baghdadi et al. 2016; Yegane Badi et al. 2018; Lompe et al. 2018).

In that sense, the overall objective of this work was to use primary sludge from the pulp and paper industry as precursor to produce an efficient waste-based MAC for the adsorption of the antiepileptic CBZ from wastewater. The production of a MAC that combines high CBZ adsorption efficiency with immediate magnetic separation from the treated aqueous phase, was here optimized. Additionally, the relationship between the produced magnetic adsorbents' physical and chemical characterization and their performance was a key objective of this study.

2. Experimental section

2.1 Production of waste-based powdered activated carbon

Primary sludge from pulp and paper mill industry (PS), a cellulosic solid residue, was used as precursor for the preparation of a waste-based powdered activated carbon (WPAC). The procedure was selected according to optimal conditions determined by Jaria et al. (2019). A schematic representation of this procedure is provided in Scheme 1. Briefly, PS was collected from a pulp and paper factory, using eucalyptus wood (*Eucalyptus globulus*) as raw material and an elemental chlorine free bleaching method. After drying, PS was ground with a blade mill and

chemically activated with KOH 1:1 (*w/w*) for 1 h under ultrasonic agitation, at room temperature. Batches of 15 g of PS were impregnated with 15 g of KOH in 50 mL of distilled water. The slurry was then allowed to dry at room temperature in the fume hood under weak air stream flow. The impregnated material was subsequently pyrolyzed in porcelain crucibles at 800 ºC in a convection furnace muffle for 150 min with a heating rate of 10 ºC min^{-1}, under constant nitrogen flow through the entire process. After pyrolysis, the carbonized material was acid washed using 1.0 M HCl in a 3% (*w/v*) proportion for 1 h. The mixture was vacuum filtered through a 0.45 µm filter to remove the acid and successively washed with distilled water and filtered until the filtrate reached neutral pH. The WPAC was dried at 100 ºC overnight and ground into a homogenous powder using a pestle and mortar.

2.2 Production of magnetic activated carbon

The WPAC was impregnated with magnetic iron oxides, namely magnetite and maghemite, to produce magnetic waste-based powdered activated carbons, through *in-situ* coprecipitation (Scheme 1). Briefly, magnetic particles were synthesized from an aqueous iron salt solution (Fe^{3+} and Fe^{2+}) through the addition of a base to a mixture of iron salts and WPAC under inert atmosphere. For that purpose, a mixture of $FeCl_3.6H_2O$:$FeSO_4.1.5H_2O$ (1:2 *w/w*) was dissolved in 50 mL of previously deoxygenized water under N_2 flux, at 70-80 ºC. A defined mass of WPAC was added after complete dissolution. An alkali solution of 0.5 M KOH (50 mL), prepared with deoxygenized water, was added dropwise and the reaction was held during 1 h, keeping the temperature at 70-80 ºC. The produced MAC was magnetically decanted to remove the excess of alkali solution and washed successively with distilled water until neutral pH, after which the particles were dried in a convection oven at 40 ºC, overnight or until completely dry, and mechanically ground. Also, magnetic particles without activated carbon (MP1) and a MAC (MCAC2) from a commercial PAC (PBFG4, ChemViron) were produced. Magnetic separation

161 from solution was performed using a neodymium rod shaped magnet (1 cm diameter; 4 cm
162 height; 1.26-1.29 T). Table 1 lists all the materials studied in this work, indicating the sources of
163 the materials and the different mass ratios of the non-magnetic activated carbon precursors to
164 iron salt mixture used to produce each adsorbent.
165
166 **2.3 Materials characterization**
167 **2.3.1 Total organic carbon**
168 Total organic carbon (TOC) was determined by calculating the difference between total carbon
169 (TC) content and inorganic carbon (IC) content, both determined with a TOC analyser (Shimadzu,
170 TOC-VCPH solid sample module SSM-5000A, Japan). Samples were analysed in triplicate and the
171 carbon content was obtained by the average of such measurements.
172 **2.3.2 Fourier transform infrared spectroscopy with attenuated total reflectance**
173 The FTIR-ATR spectra were recorded on a FTIR spectrophotometer (Shimadzu, IRaffinity-1,
174 Japan), using an attenuated total reflectance (ATR) module, with a nitrogen purge, between 700-
175 4000 cm^{-1} for PS and WPAC and 400-4000 cm^{-1} for MAC and MP1, 4.0 of resolution, 128 scans
176 and with atmosphere and background correction.
177 **2.3.3 Specific surface area and pore morphology**
178 Physical textural properties were evaluated on a surface area and porosity analyser
179 (Micromeritics, Gemini VII 2380, USA) by nitrogen adsorption isotherms at -196 ºC, after sample
180 degasification overnight at 120 ºC. The following parameters were determined: specific surface
181 area (S_{BET}) was calculated by the Brunauer-Emmett-Teller equation (Brunauer et al. 1938) in the
182 relative pressure range 0.01-0.1; total micropore volume (W_0) was determined by the Dubinin-
183 Radushkevich equation (Marsh and Rand 1970); total pore volume (V_p) was estimated from the
184 amount of nitrogen adsorbed at a relative pressure of 0.99; average pore width (D) was
185 calculated as $D = 2 \times V_p/S_{BET}$ (Calisto et al. 2014).
186

2.3.4 Scanning electron microscopy

Superficial morphology was analysed through scanning electron microscopy (SEM) images, which were obtained using a scanning electron microscope (Hitachi, S4100, Japan) at magnifications of 100x, 500x, 3000x, 10 000x and 50 000x. Prior to the SEM analysis, the samples were covered with a thin layer of carbon and an electron acceleration voltage of 20 kV was applied.

2.3.5 Point of zero charge

The point of zero charge (PZC) was determined by the pH drift method, similarly to Jaria et al. (2015). A set of ten different pH solutions (pH_i = 2-11) of 0.1 M NaCl were prepared, and initial pH (pH_i) values were adjusted with 0.1 M and 0.01 M HCl, and 0.1 M and 0.01 M NaOH. 1 mg of material was incubated in 40 mL of each pH solution (25 mg L^{-1}), in propylene tubes for 24 h at 25 ºC, in an overhead shaker. The final pH (pH_f) was measured and the PZC was determined by plotting ΔpH (pH_f – pH_i) versus pH_i. The PZC is the pH value corresponding to the *x*-axis interception of the obtained curve.

2.3.6 Vibrating sample magnetometer

The magnetization measurements were performed using a vibrating sample magnetometer (VSM EV9) with an applied magnetic field (*H*) to a maximum of 22 kOe. Sample saturation magnetization (M_S) was determined by plotting magnetic moment *versus* applied magnetic field, the M_S corresponded to the plateau value of the magnetization. The sample (about 10 mg) was encapsulated in an acrylic cylindrical container (5.85 mm of diameter and 2.60 mm of height), which was coupled to the lineal motor of the VSM EV9 instrument, centred between the two polar heads of the electromagnet used to provide the magnetic field. Prior to the analysis, the instrument was calibrated with a disk of pure nickel (8 mm of diameter) using a procedure that establishes the determination of the magnetic field, applied at around 1 Oe, while the dispersion of the magnetic moment (*m*) is inferior to 0.5 %.

2.3.7 X-ray diffraction

X-ray diffraction (XRD) analysis was performed to evaluate the presence of magnetic iron oxides in the produced materials. Measurements were performed at room temperature with a PANalytical Empyrean powder diffractometer using monochromated CuKα radiation (λ = 1.541º A) in the 10-80º 2θ range at 0.02º resolution, and 4000 acquisition points per step. The incident beam optics included a Soller slit of 0.04 rad, a 10 mm fixed mask, a divergence fixed slit of 1=4 and an anti-scatter slit of 1=8. The diffracted beam optics included a Soller slit of 0.04 rad and anti-scatter slit of 7.5 mm.

2.4 Batch adsorption experiments

The adsorptive performance of the produced materials was evaluated by batch adsorption tests. Succinctly, the adsorbent materials were weighed in a microbalance, with an uncertainty of ± 0.001 mg, added to propylene tubes with 40 mL of 5 mg L^{-1} CBZ solution and shaken, at 80 rpm, in an overhead shaker, at 25 ºC. All experiments were replicated three times along with CBZ solutions shaken without adsorbent, which were used as controls. After the corresponding shaking period, the adsorbent was separated from the aqueous phase, which was analysed for the residual CBZ concentration.

Preliminary CBZ adsorption tests in ultrapure water were performed to assist in the selection of the most efficient MAC, which was further studied through kinetic and isothermal adsorption experiments. For this purpose, fixed doses of each material (25 and 50 mg L^{-1}) were shaken in triplicate with 40 mL of 5 mg L^{-1} CBZ solution during 24 h and were then analysed for the residual CBZ concentration. According to the preliminary adsorptive performance obtained with these tests, one MAC was selected, further characterized (the PZC of this material was determined as described in section 2.3.5) and used for kinetic and equilibrium adsorption studies that were carried out both in ultrapure and WWTP effluent (as next described in sections 2.4.1 and 2.4.2). The WWTP effluent used in this work was gathered at a local urban WWTP (Aveiro, Portugal) that receives an average wastewater flow of 39 278 m^3 per day, which is subjected to primary

239 followed by biological treatment. Immediately after collection, the effluent was vacuum filtered
240 through a 0.45 µm Supor-450 Cellulose Membrane Disc Filter, in order to remove suspended
241 organic matter and solid residues. Then, the filtered effluent was stored at 4 ºC in the dark until
242 use, within a maximum of three weeks. WWTP effluent pH (Hanna Instruments, HI2020-02 pH
243 meter), conductivity (WTW meter) and dissolved organic carbon (DOC) (Shimadzu, TOC-VCPH
244 liquid sample module SSM-5000A, Japan) were measured. The determined values were pH =
245 8.07, conductivity = 2.77 mS cm^{-1} and DOC = 19.4 ± 0.3 mg L^{-1}. These characteristics are coherent
246 with previous collections from the same WWTP used in the work of Silva et al. (2019) (who
247 studied the adsorption of three pharmaceuticals, including CBZ), which validates future
248 comparisons.
249
250 **2.4.1 Kinetic adsorption study**
251 The kinetic study, carried out with the selected MAC, involved shaking a fixed concentration of
252 adsorbent material for different periods of time. In that sense, and based on preliminary
253 experiments, 25 mg L^{-1} was established as the fixed concentration of material, in both ultrapure
254 water and WWTP effluent. Accordingly, 40 mL of a 5 mg L^{-1} CBZ solution was shaken with the
255 referred fixed amount of MAC for 5, 10, 15, 30, 60 and 120 minutes in ultrapure water and 5,
256 10, 15, 30, 60, 120 and 240 minutes in WWTP effluent. The amount of CBZ adsorbed at each
257 time (q_t (mg g^{-1})) was determined by Equation (1):

258 $$q_t = \frac{(C_0 - C_t)V}{m} \quad (1)$$

259 where C_0 (mg L^{-1}) is the initial concentration of pharmaceutical, C_t (mg L^{-1}) is the pharmaceutical
260 concentration at time t (mg L^{-1}), V is the volume of solution (L) and m is the mass of adsorbent
261 (g).
262 The kinetic experimental results were fitted to the pseudo-first and pseudo-second order
263 models (Equations (2) (Lagergren 1898) and (3) (Ho and McKay 1999), respectively).

264 $$q_t = q_e[1 - exp(-k_1 t)] \quad (2)$$

$$q_t = \frac{k_2 q_e^2 t}{1 + k_2 q_e t} \quad (3)$$

where k_1 (min^{-1}) and k_2 (g mg^{-1} min^{-1}) are the pseudo-first and pseudo-second order rate constant, respectively, q_e (mg g^{-1}) is the fitted CBZ adsorbed concentration at equilibrium and q_t (mg g^{-1}) is the adsorbed concentration at a certain time. Non-linear fittings were determined using Graph Pad Prism 5 software. Three parameters (coefficient of determination (R^2), standard deviation of residuals ($S_{y/x}$) and absolute sum-of-squares (ASS)) were used to evaluate the adequacy of the model fitting, as described in section 1 of SM (SM1).

2.4.2 Equilibrium adsorption study

The equilibrium study involved shaking different concentrations of the selected adsorbent material during a time that guarantees the equilibrium of adsorption, as inferred from kinetic results. In that sense, the material was shaken for 2 h in ultrapure water and 4 h in WWTP effluent (ensuring the attainment of equilibrium) together with 40 mL of a 5 mg L^{-1} CBZ solution. The CBZ adsorbed concentration at equilibrium q_e (mg g^{-1}) was determined as defined by Equation (1), but respectively replacing q_t (mg g^{-1}) and C_t (mg L^{-1}) by q_e (mg g^{-1}) and C_e (mg L^{-1}) (the aqueous phase concentration of pharmaceutical at equilibrium), considering that the equilibrium has been reached. Experimental data were fitted to the Langmuir and Freundlich non-linear equilibrium models, mathematically represented by Equations (4) (Langmuir 1918) and (5) (Freundlich 1906) respectively:

$$q_e = \frac{q_m K_L C_e}{1 + K_L C_e} \quad (4)$$

$$q_e = K_F C_e^{1/n} \quad (5)$$

where K_L (L mg^{-1}) is the Langmuir equilibrium constant, K_F (mg$^{1-1/n}$ L$^{1/n}$ g^{-1}) is the Freundlich equilibrium constant and n is a constant related with non-linearity of the equation. Non-linear fittings were determined using Graph Pad Prism 5 software. Three fitting parameters (R^2, $S_{y/x}$ and ASS) were used to evaluate the adequacy of the model fitting (SM1).

290

291 **2.5 Analytical method**

292 The quantification of CBZ was performed by Micellar Electrokinetic Chromatography (MEKC) in
293 a Beckman P/ACE MDQ (Fullerton, CA, USA) equipped with a photodiode array UV-Vis detector,
294 using the software 32 Karat. The separation method was operated in a dynamically coated fused
295 silica capillary with 40 cm total length, 30 cm to the detection window, 75 µm of internal
296 diameter, as described in Calisto et al. (2015). Ethylvanillin was used as internal standard and a
297 15 mM sodium tetraborate and 20 mM SDS solution was used as running buffer, prepared fresh
298 every two days and stored at 4 ºC. A 100 mM sodium tetraborate solution was used as
299 electrolyte and added to each sample along with internal standard. CBZ detection was
300 performed at 214 nm and samples' concentration was determined in triplicate using a
301 calibration curve with seven standard solutions with concentrations in the range of 0.25 to 5.0
302 mg L^{-1}. Each standard was analysed in quadruplicate and a new calibration curve was obtained
303 for every new capillary. All buffers and CBZ standards were prepared in ultrapure water (Milli-
304 Q, Merck Millipore). Complementary information about sample preparation and the separation
305 method used can be consulted in SM2. Peak integration was performed with Matlab 7.0
306 software.

307

308 **3. Results and discussion**

309 **3.1 Materials characterization**

310 Figure 1 represents TOC and IC contents of the here considered carbon-based materials.
311 According to TOC determinations (Figure 1), pyrolysis strongly contributes to its increase, as
312 proved by the 40% increment when comparing WPAC with PS. As may be seen in Figure 1, IC
313 content is residual, approximately 0.03-0.12%, for WPAC and all produced MAC, which reflects
314 its efficient removal during the HCl washing step. The TOC decrease in MAC, whether waste- or
315 commercial-based, is evident and in proportion to the iron fraction in the composite (Table 1).

316 Results from FTIR analysis are shown in Figure S2, within SM3. The FTIR spectrum of PS (Figure
317 S2-a)) displays specific peaks around 1430 cm^{-1} and 870 cm^{-1}, which are indicators of the
318 presence of carbonate groups. These peaks are clearly absent in WPAC spectrum (Figure S2-b))
319 corroborating IC results. Aromatic ring deformation vibration and C-C stretching can be
320 correlated with the peaks at 700-750 cm^{-1}, the peak at around 1650 cm^{-1} can be associated with
321 aromatic C=C stretch and aliphatic C-H stretching signals can also be deduced from the band in
322 the 2815-3000 cm^{-1} range (Marsh and Rodríguez-Reinoso 2006; Sevilla and Fuertes 2009).
323 Regarding the presence of oxygen groups, the broad band (3000-3700 cm^{-1}) centred at 3330 cm^{-1}, in addition to a peak at 2930 cm^{-1}, might be attributed to alcohol/phenol O-H stretching
325 vibrations, the peak at around 1100 cm^{-1} is often associated with the C-O-C stretch characteristic
326 of ether groups (Stuart 2004). In the WPAC and MAC spectra, the intensity abatement of the
327 peaks at 1000-1250 cm^{-1} and the broad band at 3000-3700 cm^{-1} can be associated with
328 dehydration during the pyrolysis of the highly cellulosic PS (Sevilla and Fuertes 2009).
329 Nonetheless, still may be inferred the presence of oxygen containing groups such as phenol,
330 carboxyl and hydroxyl groups as well as some indications of the aromaticity of WPAC at 1430-
331 1650 cm^{-1} (Stuart 2004). Broad bands at 540 cm^{-1} and peaks at 650 cm^{-1} can be linked with Fe-O
332 bonds compatible with the presence of magnetite and maghemite (Cornell and Schwertmann
333 2003; Mohan et al. 2011).
334 Figure 2 displays the XRD patterns of WPAC, MP1 and MAC4. Activated carbons are
335 characterized by their amorphous structure composed by non-graphitic and non-graphitizable
336 carbon, without any measurable crystallographic order. However, some intermediate structures
337 between graphite and amorphous state (turbostratic structures) can be deduced from the XRD
338 pattern of WPAC – peaks at 28.2° and 47.5° (Balachandran and Ag 2012). Additionally, peaks at
339 around 33.0° and 56.1° can be associated with potassium compounds, due to KOH activation,
340 and some oxygen groups, respectively (Mopoung et al. 2015). A characteristic XRD pattern with
341 diffraction peaks at 30.2°, 35.4°, 43.2°, 53.5°, 57.1° and 62.8°, is associated with the cubic spinel

342 structure of magnetite and maghemite (Cornell and Schwertmann 2003). This pattern is found
343 in both XRD spectra of MP1 and MAC4. The distinction between the two magnetic iron oxide is
344 not possible by XRD but it is possible to state that magnetite and/or maghemite are the two
345 main crystalline components present.
346 Results on the textural and magnetic properties of the materials are depicted in Table 2.
347 Regarding the S_{BET}, that of WPAC is 1533 $m^2 g^{-1}$ (Table 2), which is consistent with previous works
348 (Silva et al. 2019; Jaria et al. 2019) and within typical values for PAC. In fact, the S_{BET} of WPAC is
349 considerably higher than that of the commercial PBFG4 (Calisto et al. 2014), revealing the
350 potentiality of this waste-based adsorbent. The results from Table 2 highlighted that the
351 introduction of iron oxide nanoparticles in the carbon matrix of WPAC negatively affected the
352 S_{BET} of the produced MAC. Besides, the reduction of S_{BET} values of MAC is in agreement with the
353 increase of iron salt content in the materials (Table 1). This can be explained by the relatively
354 low S_{BET} of the bare MP1 nanoparticles and their occupation of the interstitial spaces of the
355 porous structure of WPAC, causing a decrease in the overall S_{BET} of MAC. The reverse relation is
356 observed for the M_S values, which in the case of MAC6 is identical to the result of the MP1
357 particles. All the produced MAC have M_S values ranging between 22.8 and 56.4 emu g^{-1}, which
358 assure successful retrievability from an aqueous medium using a permanent magnet. However,
359 considering visual responsiveness, complete and more immediate magnetic separation was
360 attained by MAC3, MAC4 and MAC6. From Table 2, it is also possible to infer the highly
361 microporous structure of WPAC as the micropore volume (W_0) accounts for approximately 58%
362 of total pore volume (V_p). Although MAC average pore diameter (D) results are, in general,
363 compatible with a microporous structure (< 2 nm), V_p and W_0 were reduced in comparison with
364 WPAC by the presence of MP1 in the composite. Due to the nanometric size of the magnetic
365 iron oxide particles produced through alkaline coprecipitation (Ahn et al. 2012), the referred
366 occupation of interstitial pore spaces is confirmed by the significant reduction of W_0 with the
367 increasing proportion of iron salt, and therefore MP1 content, in MAC. This can be also inferred

368 when comparing the properties of MCAC2 with its precursor PBFG4 since MCAC2 and PBFG4
369 have similar V_p but the W_0 of PBFG4 is significantly reduced after magnetization.
370 SEM images, which are presented in Figure 3 and Figure S3, provide visual context for the results
371 in Table 2. MAC surfaces are rougher than the precursor WPAC (Figure S3) due to the deposition
372 of magnetic particles throughout the carbon surface and is clear that increasingly iron salt
373 proportions correspond to rougher surfaces and increasingly pore constraints. The
374 amplifications at 50 000x, particularly in the case of MAC3, MAC4 and MAC6, clearly depict the
375 pore constraints in the basis of the poorer textural properties of MAC.
376

377 **3.2 Batch adsorption experiments**

378 Figure 4 and Table S1 present the results for the preliminary tests performed at 25 mg L^{-1} and 50
379 mg L^{-1} of material dosage. As it can be observed, the non-magnetized materials, namely PBFG4
380 and WPAC, mostly showed higher CBZ removal percentages than any of the magnetic carbons
381 at both dosages. Indeed, WPAC performed better than PBFG4 in the adsorption of CBZ, which
382 may be related to the higher S_{BET} of the first (Table 2). Meanwhile, MP1 was not able to remove
383 any CBZ from water (please see Table S1). Regarding the MAC (MAC2 to MAC6), the CBZ removal
384 percentages ranged between 15 and 50 % at 25 mg L^{-1} and between 36 and 91 at 50 mg L^{-1}. At
385 both dosages, the lower the iron content in the material, the higher the CBZ removal percentage,
386 which can be explained by S_{BET} reduction (Table 2) and increasing pore constraints (Figure 3 and
387 Figure S3) with increasing iron content. In any case, it is important to state that, compared with
388 MCAC2, not only MAC2, which has the same iron content, but all the produced MAC revealed
389 higher or comparable removal results (Figure 4 and Table S1).
390 Taking into account the results presented above concerning preliminary adsorption tests in
391 ultrapure water, MAC4 was selected for further adsorption studies because this material
392 revealed the best relation between CBZ adsorption performance and immediate magnetic
393 separation. Accordingly, the PZC of MAC4 was determined (PZC ~ 6, please see Figure S4) and

394 both kinetic and equilibrium studies were performed using MAC4 for the adsorption of CBZ from
395 ultrapure water and from the WWTP effluent.
396
397 **3.3.4 Kinetic adsorption study**
398 The determination of the equilibrium time is paramount when studying the viability of an
399 industrial application of an adsorbent material. Apart from good adsorptive performance, the
400 period required to attain equilibrium, and hence maximum performance, must allow
401 applicability. The kinetic studies were performed to determine the adsorption rate and the
402 equilibrium time (t_e), which is the time required for the CBZ to reach the equilibrium at the
403 interface between the bulk solution and the surface of the adsorbent. Figure 5 presents the
404 experimental data on the adsorbed concentration of CBZ *versus* the contact time together with
405 model fittings for MAC4 in ultrapure and wastewater. From the analysis of the kinetic curves,
406 the t_e in ultrapure water is around 15-30 minutes and around 45-60 minutes in WWTP effluent.
407 Considering that some adsorption systems present equilibrium times of several hours (To et al.
408 2017; Delgado et al. 2019), this feature reveals the kinetic suitability of this magnetic material
409 for CBZ adsorption.

410 Kinetic model fitting parameters are summarized in Table 3. Considering the statistical analysis,
411 the pseudo-first and pseudo-second model fittings presented R^2 values above 0.98, which
412 indicates that both models reasonably describe the experimental data in ultrapure water and
413 WWTP effluent. As for WPAC, previous results [34], which were included in Table 3 for
414 comparison purposes, revealed that experimental data obtained in both matrices are better
415 described by the pseudo-second model. According to the kinetic rate constants ($k_1$and k_2), the
416 MAC4 presents faster CBZ adsorption kinetics than the precursor WPAC (data presented in Table
417 3) either in ultrapure water or WWTP effluent. Apart from that, and contrarily to WPAC [34], the
418 adsorption of CBZ onto MAC4 is negatively affected in the WWTP effluent, where it is
419 approximately 10 times slower (please see k_2 values in Table 3). This might be attributed to the

DOC pore blockage and competition for adsorption sites, which can slow down adsorption kinetics (Li et al. 2003; Altmann et al. 2014; Shimabuku et al. 2014).

3.3.5 Equilibrium adsorption study

CBZ adsorption equilibrium studies were performed using MAC4 in ultrapure water and WWTP effluent. Figure 6 displays the graphical representation of the adsorbed concentration of CBZ onto MAC4 at equilibrium (q_e, mg g^{-1}) *versus* the CBZ remaining concentration in solution (C_e, mg L^{-1}) in both matrices. The isotherm model fitting parameters are summarized in Table 3. From the analysis of R^2, ASS and $S_{y/x}$, it is possible to conclude that the Langmuir and Freundlich isotherm models adequately outline the experimental data in both matrices ($R^2 > 0.96$). Hence, both models can be used to draw comparisons. The same was already verified for the non-magnetic WPAC [34], with the Langmuir model providing slightly better fittings (Table 3).

The results show that the non-magnetic WPAC presents better performance than MAC4 for CBZ adsorption in ultrapure water and WWTP effluent. In ultrapure water, the Langmuir maximum adsorption capacity (q_m) of MAC4 (68 ± 4 mg g^{-1}) for CBZ is about 3 times lower when compared to the q_m of WPAC (212 ± 16 mg g^{-1}) determined by Silva et al. (2019). This q_m reduction must be related with the materials S_{BET}. Note that the S_{BET} of MAC4 (551 m^2 g^{-1}) is approximately 3 times lower than that of the WPAC used by Silva et al. (2019) (1627 m^2 g^{-1}). The same relation is verified when comparing both materials in wastewater matrix.

Obtained results on the adsorption of CBZ onto MAC4 may be related with electrostatic interactions since, in the adsorption process, the protonation state of the adsorbate and adsorbent's surface, dictated by the pH of the aqueous matrix, is a decisive factor. Considering that the PZC of MAC4 is around 6 (Figure S4), its surface is mainly deprotonated and negatively charged in the tested conditions (WWTP effluent pH=8.07; ultrapure water pH=5.5-6.0).

444 Regarding the protonation state of CBZ and considering its pk_a values (pk_{a1}=2.3 (Nghiem et al.
445 2005) and pk_{a2}=13.9 (Jones et al. 2002)), it is expected neutral net charge under the tested
446 conditions. Hence, no electrostatic repulsion forces occur between the surface of MAC4 and the
447 neutral CBZ. Corroborating this hypothesis, the results from Table 3 highlight that the matrix
448 type has little interference on the adsorption of CBZ onto MAC4, with the adsorption capacities
449 being mostly equal in ultrapure water and WWTP effluent.

450 The decline in the adsorptive performance verified when comparing the non-magnetic precursor
451 with the magnetic adsorbent is inevitable and inherent to the introduction of the magnetic iron
452 oxide particles (Baghdadi et al. 2016). In any case, when compared with maximum adsorption
453 capacities of several non-magnetic adsorbents used in the literature for the adsorption of CBZ
454 (Delhiraja et al. 2019; Turk Sekulic et al. 2019; Kebede et al. 2019), which are presented in Table
455 4, MAC4 performs well.

456 Very few studies report on the application of MAC in the removal of CBZ from water (Shan et al.
457 2016; Wong et al. 2016; Baghdadi et al. 2016), which have been included in Table 4. It is the case
458 of Shan et al. (2016), using a waste-based MAC (S_{BET} = 486 m^2 g^{-1}; M_S = 20.8 emu g^{-1}) for CBZ
459 adsorption in ultrapure water. This study determined an adsorption capacity of 135.1 mg g^{-1} for
460 the magnetic adsorbent and an equilibrium time of 10 h. Apart from the present study, the work
461 of Baghdadi et al. (2016) is, to the best of the author's knowledge, the only study reporting on
462 the adsorption capacity of a MAC for the removal of CBZ in wastewater. The MAC used was
463 obtained from a commercial activated carbon and presented great surface area (S_{BET} = 1241 m^2
464 g^{-1}) which translated into a great adsorption capacity (q_m=182.9 mg g^{-1}), mostly explained by the
465 reduced mass fraction of magnetite nanoparticles in the composite and a concomitant reduction
466 of the magnetization of the composite (M_S = 5.06 emu g^{-1}) (Baghdadi et al. 2016). The challenge
467 in the production of MAC is finding the right compromise between adsorption capacity and
468 immediate and efficient recoverability from the aqueous matrix. Although with inferior

performance when compared to other MAC in Table 4, the here produced MAC4 is readily and effectively separated from solution (M_S = 39.84 emu g^{-1}, Table 2) which was a key objective of this study. Significantly, this work provides a pathway for the upcycling of a cellulosic industrial waste into an added-value product with application in the removal of pharmaceuticals from water which enforces the principles of a circular economy. Future works include further optimization of the production with the intent of minimizing the negative effect of the magnetic nanoparticles in the adsorptive performance while assuring successful recuperation from the aqueous matrix. Nonetheless, the results provide a promising insight on the potential application of a waste-based MAC in the removal of CBZ from real WWTP effluents.

4. Conclusions

In this study, a waste-based MAC was successfully produced from primary sludge from the pulp and paper industry via an *in-situ* coprecipitation of magnetic iron oxides, and applied in the removal of CBZ from ultrapure water and WWTP final effluent. The impartment of magnetic properties to the WPAC resulted in poorer textural characteristics, namely surface area and micropore volume (S_{BET}, W_0), resulting from pore blockage, as confirmed by SEM analysis, and from the introduction of the inactive magnetic mass fraction (low S_{BET}). This was considered the main factor leading to the decrease in the adsorptive performance verified for all produced MAC in comparison to their precursor. The selected MAC4 (S_{BET} = 551 m^2 g^{-1}) combined immediate and efficient magnetic retrievability (M_S = 39.84 emu g^{-1}) with good CBZ removal percentage. The kinetic studies of MAC4 revealed very short equilibrium times in ultrapure water (15-30 min) and in WWTP effluent (45-60 min), even shorter than those determined for the precursor WPAC. According to the maximum adsorption capacities determined by the Langmuir adsorption model, the q_m of MAC4 in both ultrapure and wastewater was approximately 3 times lower than that of WPAC, mostly due to S_{BET} differences. Matrix effects were not significant when comparing

494 the q_m results for MAC4 in ultrapure water and WWTP effluent (68 ± 4 and 60 ± 3 mg g^{-1},
495 respectively), which is a favourable result in view of the practical application of MAC4 for the
496 tertiary treatment of wastewater. Overall, this study points the potential of MAC4 in the removal
497 of CBZ from WWTP final effluents and represents a step forward towards the application of
498 magnetically retrievable waste-based activated carbons in continuous WWTP tertiary treatment
499 systems for the adsorption of pharmaceuticals.

500

501 **5. Acknowledgements**

502 This work is a contribution to the project WasteMAC (POCI-01-0145-FEDER-028598) funded by
503 FCT – Fundação para a Ciência e a Tecnologia, I.P., through national funds, and the co-funding
504 by the FEDER, within the PT2020 Partnership Agreement and Compete 2020. Thanks are also
505 due for the financial support to CESAM (UID/AMB/50017/2019), to FCT/MCTES through national
506 funds, and the co-funding by the FEDER, within the PT2020 Partnership Agreement and Compete
507 2020. Marta Otero and Diogo Pereira thank FCT funding through IF Program (IF/00314/2015).
508 Vânia Calisto is thankful to FCT for the Scientific Employment Stimulus support
509 (CEECIND/00007/2017). María V. Gil acknowledges support from a Ramón y Cajal grant (RYC-
510 2017-21937) of the Spanish government, co-financed by the European Social Fund (ESF).

511

512 **References**

513 Ahn T, Kim JH, Yang HM, et al (2012) Formation pathways of magnetite nanoparticles by
514 coprecipitation method. J Phys Chem C 116:6069–6076.
515 https://doi.org/10.1021/jp211843g

516 Altmann J, Ruhl AS, Zietzschmann F, Jekel M (2014) Direct comparison of ozonation and
517 adsorption onto powdered activated carbon for micropollutant removal in advanced
518 wastewater treatment. Water Res 55:185–193.
519 https://doi.org/http://dx.doi.org/10.1016/j.watres.2014.02.025

520 Baghdadi M, Ghaffari E, Aminzadeh B (2016) Removal of carbamazepine from municipal
521 wastewater effluent using optimally synthesized magnetic activated carbon: Adsorption
522 and sedimentation kinetic studies. J Environ Chem Eng 4:3309–3321.
523 https://doi.org/10.1016/j.jece.2016.06.034

524 Bahlmann A, Brack W, Schneider RJ, Krauss M (2014) Carbamazepine and its metabolites in
525 wastewater: Analytical pitfalls and occurrence in Germany and Portugal. Water Res
526 57:104–14. https://doi.org/10.1016/j.watres.2014.03.022

527 Balachandran M, Ag K (2012) Study of Stacking Structure of Amorphous Carbon by X-Ray
528 Diffraction Technique. Int J Electrochem Sci 7:3127–3134

529 Bayramoglu G, Arica MY (2018) Adsorption of Congo Red dye by native amine and carboxyl
530 modified biomass of Funalia trogii: Isotherms, kinetics and thermodynamics mechanisms.
531 Korean J Chem Eng 35:1303–1311. https://doi.org/10.1007/s11814-018-0033-9

532 Bayramoglu G, Arica MY, Liman G, et al (2016) Removal of bisphenol A from aqueous medium
533 using molecularly surface imprinted microbeads. Chemosphere 150:275–284.
534 https://doi.org/https://doi.org/10.1016/j.chemosphere.2016.02.040

535 Bayramoglu G, Kunduzcu G, Arica MY (2020) Preparation and characterization of strong cation
536 exchange terpolymer resin as effective adsorbent for removal of disperse dyes. Polym
537 Eng Sci 60:192–201. https://doi.org/10.1002/pen.25272

538 Boehler M, Zwickenpflug B, Hollender J, et al (2012) Removal of micropollutants in municipal
539 wastewater treatment plants by powder-activated carbon. Water Sci Technol 66:2115–
540 2121. https://doi.org/10.2166/wst.2012.353

541 Brunauer S, Emmett PH, Teller E (1938) Adsorption of Gases in Multimolecular Layers. J Am
542 Chem Soc 60:309–319. https://doi.org/10.1021/ja01269a023

543 Calisto V, Esteves VIVI (2009) Psychiatric pharmaceuticals in the environment. Chemosphere
544 77:1257–1274. https://doi.org/10.1016/j.chemosphere.2009.09.021

545 Calisto V, Ferreira CIA, Santos SM, et al (2014) Production of adsorbents by pyrolysis of paper
546 mill sludge and application on the removal of citalopram from water. Bioresour Technol
547 166:335–344. https://doi.org/10.1016/j.biortech.2014.05.047

548 Calisto V, Ferreira CIACIA, Oliveira JABPJABP, et al (2015) Adsorptive removal of
549 pharmaceuticals from water by commercial and waste-based carbons. J Environ Manage
550 152:83–90. https://doi.org/http://dx.doi.org/10.1016/j.jenvman.2015.01.019

551 Cazetta AL, Vargas AMM, Nogami EM, et al (2011) NaOH-activated carbon of high surface area
552 produced from coconut shell: Kinetics and equilibrium studies from the methylene blue
553 adsorption. Chem Eng J 174:117–125. https://doi.org/10.1016/j.cej.2011.08.058

554 Cornell RM, Schwertmann U (2003) The Iron Oxides Structure, Properties, Reactions,
555 Occurences and Uses, 2nd Editio. Wiley-VCH

556 de Jesus Gaffney V, Almeida CMM, Rodrigues A, et al (2015) Occurrence of pharmaceuticals in
557 a water supply system and related human health risk assessment. Water Res 72:199–208.
558 https://doi.org/10.1016/J.WATRES.2014.10.027

559 Delgado N, Capparelli A, Navarro A, Marino D (2019) Pharmaceutical emerging pollutants
560 removal from water using powdered activated carbon: Study of kinetics and adsorption
561 equilibrium. J Environ Manage 236:301–308.
562 https://doi.org/10.1016/J.JENVMAN.2019.01.116

563 Delhiraja K, Vellingiri K, Boukhvalov DW, Philip L (2019) Development of Highly Water Stable
564 Graphene Oxide-Based Composites for the Removal of Pharmaceuticals and Personal
565 Care Products. Ind Eng Chem Res 58:2899–2913.
566 https://doi.org/10.1021/acs.iecr.8b02668

Deloitte Sustainability (2018) Options for a strategic approach to pharmaceuticals in the environment - Final Report

Desbiolles F, Malleret L, Tiliacos C, et al (2018) Occurrence and ecotoxicological assessment of pharmaceuticals: Is there a risk for the Mediterranean aquatic environment? Sci Total Environ 639:1334–1348. https://doi.org/10.1016/J.SCITOTENV.2018.04.351

European Commission (2015) Decision 2015/495/EU of 20 March 2015 establishing a watch list of substances for Union-wide monitoring in the field of water policy pursuant to Directive 2008/ 105/ EC of the European Parliament and of the Council. Brussels

European Commission (2018) Decision 2018/840/EU of 5 June 2018 establishing a watch list of substances for Union-wide monitoring in the field of water policy pursuant to Directive 2008/105/EC of the European Parliament and of the Council and repealing Commission Implementing Decisi. Brussels

Freundlich H (1906) Uber die Adsorption in Losungen. Zeitschrift für Phys Chemie 57:385–470

Guillossou R, Le Roux J, Mailler R, et al (2019) Organic micropollutants in a large wastewater treatment plant: What are the benefits of an advanced treatment by activated carbon adsorption in comparison to conventional treatment? Chemosphere 218:1050–1060. https://doi.org/10.1016/J.CHEMOSPHERE.2018.11.182

Hao Z, Wang C, Yan Z, et al (2018) Magnetic particles modification of coconut shell-derived activated carbon and biochar for effective removal of phenol from water. Chemosphere 211:962–969. https://doi.org/10.1016/j.chemosphere.2018.08.038

Ho Y., McKay G (1999) Pseudo-second order model for sorption processes. Process Biochem 34:451–465. https://doi.org/10.1016/S0032-9592(98)00112-5

Ioannidou O, Zabaniotou A (2007) Agricultural residues as precursors for activated carbon production—A review. Renew Sustain Energy Rev 11:1966–2005. https://doi.org/http://dx.doi.org/10.1016/j.rser.2006.03.013

Jaria G, Calisto V, Gil MV, et al (2015) Removal of fluoxetine from water by adsorbent materials produced from paper mill sludge. J Colloid Interface Sci 448:32–40. https://doi.org/10.1016/j.jcis.2015.02.002

Jaria G, Silva CP, Oliveira JABP, et al (2019) Production of highly efficient activated carbons from industrial wastes for the removal of pharmaceuticals from water—A full factorial design. J Hazard Mater 370:212–218. https://doi.org/10.1016/J.JHAZMAT.2018.02.053

Jaria G, Silva CPCP, Ferreira CIACIA, et al (2017) Sludge from paper mill effluent treatment as raw material to produce carbon adsorbents: An alternative waste management strategy. J Environ Manage 188:203–211

Jelic A, Gros M, Ginebreda A, et al (2011) Occurrence, partition and removal of pharmaceuticals in sewage water and sludge during wastewater treatment. Water Res 45:1165–1176. https://doi.org/10.1016/j.watres.2010.11.010

Jelic A, Petrović M, Barcelo D (2012) Pharmaceuticals in Drinking Water. In: Barcelo D (ed) The Handbook of Environmental Chemistry - Emerging Organic Contaminants and Human Health, vol. 20. Springer, pp 47–70

Jones OA, Voulvoulis N, Lester JN (2002) Aquatic environmental assessment of the top 25 English prescription pharmaceuticals. Water Res 36:5013–5022. https://doi.org/S0043-1354(02)00227-0 [pii]

610 Kårelid V, Larsson G, Björlenius B (2017) Pilot-scale removal of pharmaceuticals in municipal
611 wastewater: Comparison of granular and powdered activated carbon treatment at three
612 wastewater treatment plants. J Environ Manage 193:491–502.
613 https://doi.org/10.1016/J.JENVMAN.2017.02.042

614 Kebede TG, Dube S, Nindi MM (2019) Biopolymer electrospun nanofibres for the adsorption of
615 pharmaceuticals from water systems. J Environ Chem Eng 7:.
616 https://doi.org/10.1016/j.jece.2019.103330

617 Kidd KA, Blanchfield PJ, Mills KH, et al (2007) Collapse of a fish population after exposure to a
618 synthetic estrogen. Proc Natl Acad Sci 104:8897–8901.
619 https://doi.org/10.1073/pnas.0609568104

620 Lagergren S (1898) Zur theorie der sogenannten adsorption geloster stoffe. K Sven
621 Vetenskapsakademiens Handl 24:1–39

622 Langmuir I (1918) The Adsorption of Gases on Plane Surfaces of Glass, Mica and Platinum. J Am
623 Chem Soc 40:1361–1403. https://doi.org/10.1021/ja02242a004

624 Li Q, Snoeyink VL, Mariñas BJ, Campos C (2003) Pore blockage effect of NOM on atrazine
625 adsorption kinetics of PAC: The roles of PAC pore size distribution and NOM molecular
626 weight. Water Res 37:4863–4872. https://doi.org/10.1016/j.watres.2003.08.018

627 Li X, Hai FI, Nghiem LD (2011) Simultaneous activated carbon adsorption within a membrane
628 bioreactor for an enhanced micropollutant removal. Bioresour Technol 102:5319–5324.
629 https://doi.org/10.1016/j.biortech.2010.11.070

630 Lompe KM, Vo Duy S, Peldszus S, et al (2018) Removal of micropollutants by fresh and
631 colonized magnetic powdered activated carbon. J Hazard Mater 360:349–355.
632 https://doi.org/10.1016/J.JHAZMAT.2018.07.072

633 Luiz, Oliveira CA, Rios RVRA, Fabris JD, et al (2002) Activated carbon / iron oxide magnetic
634 composites for the adsorption of contaminants in water. Carbon N Y 40:2177–2183

635 Luo Y, Guo W, Ngo HH, et al (2014) A review on the occurrence of micropollutants in the
636 aquatic environment and their fate and removal during wastewater treatment. Sci Total
637 Environ 473–474:619–641.
638 https://doi.org/http://dx.doi.org/10.1016/j.scitotenv.2013.12.065

639 Mailler R, Gasperi J, Coquet Y, et al (2015) Study of a large scale powdered activated carbon
640 pilot: Removals of a wide range of emerging and priority micropollutants from
641 wastewater treatment plant effluents. Water Res 72:315–330.
642 https://doi.org/10.1016/J.WATRES.2014.10.047

643 Malchi T, Maor Y, Tadmor G, et al (2014) Irrigation of Root Vegetables with Treated
644 Wastewater: Evaluating Uptake of Pharmaceuticals and the Associated Human Health
645 Risks. Environ Sci Technol 48:9325–9333. https://doi.org/10.1021/es5017894

646 Margot J, Kienle C, Magnet A, et al (2013) Treatment of micropollutants in municipal
647 wastewater: Ozone or powdered activated carbon? Sci Total Environ 461–462:480–498.
648 https://doi.org/http://dx.doi.org/10.1016/j.scitotenv.2013.05.034

649 Marsh H, Rand B (1970) The characterization of microporous carbons by means of the dubinin-
650 radushkevich equation. J Colloid Interface Sci 33:101–116. https://doi.org/10.1016/0021-
651 9797(70)90077-9

652 Marsh H, Rodríguez-Reinoso F (2006) Activated carbon. Elsevier

McCance W, Jones OAH, Edwards M, et al (2018) Contaminants of Emerging Concern as novel groundwater tracers for delineating wastewater impacts in urban and peri-urban areas. Water Res. 146:118–133

Meinel F, Sperlich A, Jekel M (2016) Pilot-scale study of powdered activated carbon recirculation for micropollutant removal. Water Sci Technol 74:927–934. https://doi.org/10.2166/wst.2016.273

Mohan D, Sarswat A, Singh VK, et al (2011) Development of magnetic activated carbon from almond shells for trinitrophenol removal from water. Chem Eng J 172:1111–1125. https://doi.org/10.1016/J.CEJ.2011.06.054

Mopoung S, Moonsri P, Palas W, Khumpai S (2015) Characterization and Properties of Activated Carbon Prepared from Tamarind Seeds by KOH Activation for Fe(III) Adsorption from Aqueous Solution. Sci World J 2015:. https://doi.org/10.1155/2015/415961

Nakada N, Shinohara H, Murata A, et al (2007) Removal of selected pharmaceuticals and personal care products (PPCPs) and endocrine-disrupting chemicals (EDCs) during sand filtration and ozonation at a municipal sewage treatment plant. Water Res 41:4373–4382. https://doi.org/10.1016/J.WATRES.2007.06.038

Nghiem LD, Schäfer AI, Elimelech M (2005) Pharmaceutical retention mechanisms by nanofiltration membranes. Environ Sci Technol 39:7698–705

Nielsen L, Biggs MJ, Skinner W, Bandosz TJ (2014) The effects of activated carbon surface features on the reactive adsorption of carbamazepine and sulfamethoxazole. Carbon N Y 80:. https://doi.org/10.1016/j.carbon.2014.08.081

Niemuth NJ, Klaper RD (2015) Emerging wastewater contaminant metformin causes intersex and reduced fecundity in fish. Chemosphere 135:38–45. https://doi.org/10.1016/j.chemosphere.2015.03.060

Oliveira G, Calisto V, Santos SMSM, et al (2018) Paper pulp-based adsorbents for the removal of pharmaceuticals from wastewater: A novel approach towards diversification. 631–632:1018–1028

Parliament E (2013) Directive 2013/39/EU of the European Parliament and of the Council of 12 August 2013 amending Directives 2000/60/EC and 2008/105/EC as regards priority substances in the field of water policy. Off J Eur Union

Pereira AMPT, Silva LJG, Laranjeiro CSM, et al (2017) Human pharmaceuticals in Portuguese rivers: The impact of water scarcity in the environmental risk. Sci Total Environ 609:1182–1191. https://doi.org/10.1016/J.SCITOTENV.2017.07.200

Pereira AMPT, Silva LJG, Meisel LM, et al (2015) Environmental impact of pharmaceuticals from Portuguese wastewaters: Geographical and seasonal occurrence, removal and risk assessment. Environ Res 136:108–119. https://doi.org/10.1016/j.envres.2014.09.041

Pomati F, Castiglioni S, Zuccato E, et al (2006) Effects of a complex mixture of therapeutic drugs at environmental levels on human embryonic cells. Environ Sci Technol 40:2442–2447. https://doi.org/10.1021/es051715a

Rivera-Utrilla J, Sánchez-Polo M, Ferro-García MÁ, et al (2013) Pharmaceuticals as emerging contaminants and their removal from water. A review. Chemosphere 93:1268–1287. https://doi.org/http://dx.doi.org/10.1016/j.chemosphere.2013.07.059

Satayeva AR, Howell CA, Korobeinyk A V., et al (2018) Investigation of rice husk derived

696 activated carbon for removal of nitrate contamination from water. Sci Total Environ
697 630:1237–1245. https://doi.org/10.1016/J.SCITOTENV.2018.02.329

698 Serrano D, Suárez S, Lema JM, Omil F (2011) Removal of persistent pharmaceutical
699 micropollutants from sewage by addition of PAC in a sequential membrane bioreactor.
700 Water Res 45:5323–5333. https://doi.org/10.1016/j.watres.2011.07.037

701 Sevilla M, Fuertes AB (2009) The production of carbon materials by hydrothermal
702 carbonization of cellulose. Carbon N Y 47:2281–2289.
703 https://doi.org/10.1016/j.carbon.2009.04.026

704 Shan D, Deng S, Zhao T, et al (2016) Preparation of ultrafine magnetic biochar and activated
705 carbon for pharmaceutical adsorption and subsequent degradation by ball milling. J
706 Hazard Mater 305:156–163. https://doi.org/10.1016/j.jhazmat.2015.11.047

707 Shimabuku KK, Cho H, Townsend EB, et al (2014) Modeling Nonequilibrium Adsorption of MIB
708 and Sulfamethoxazole by Powdered Activated Carbon and the Role of Dissolved Organic
709 Matter Competition. Environ Sci Technol 48:13735–13742.
710 https://doi.org/10.1021/es503512v

711 Silva CP, Jaria G, Otero M, et al (2019) Adsorption of pharmaceuticals from biologically treated
712 municipal wastewater using paper mill sludge-based activated carbon. Environ Sci Pollut
713 Res 26:13173–13184. https://doi.org/10.1007/s11356-019-04823-w

714 Silva CP, Jaria G, Otero M, et al (2018) Waste-based alternative adsorbents for the remediation
715 of pharmaceutical contaminated waters: Has a step forward already been taken?
716 Bioresour Technol 250:888–901

717 Stuart BH (2004) Infrared Spectroscopy: Fundamentals and Applications. Wiley

718 To MH, Hadi P, Hui CW, et al (2017) Mechanistic study of atenolol, acebutolol and
719 carbamazepine adsorption on waste biomass derived activated carbon. J Mol Liq
720 241:386–398. https://doi.org/10.1016/j.molliq.2017.05.037

721 Turk Sekulic M, Boskovic N, Milanovic M, et al (2019) An insight into the adsorption of three
722 emerging pharmaceutical contaminants on multifunctional carbonous adsorbent:
723 Mechanisms, modelling and metal coadsorption. J Mol Liq 284:372–382.
724 https://doi.org/10.1016/j.molliq.2019.04.020

725 Vasquez MI, Lambrianides A, Schneider M, et al (2014) Environmental side effects of
726 pharmaceutical cocktails: What we know and what we should know. J Hazard Mater
727 279:169–189. https://doi.org/10.1016/j.jhazmat.2014.06.069

728 Wong KT, Yoon Y, Snyder SA, Jang M (2016) Phenyl-functionalized magnetic palm-based
729 powdered activated carbon for the effective removal of selected pharmaceutical and
730 endocrine-disruptive compounds. Chemosphere 152:71–80.
731 https://doi.org/10.1016/J.CHEMOSPHERE.2016.02.090

732 Yegane Badi M, Azari A, Pasalari H, et al (2018) Modification of activated carbon with magnetic
733 Fe3O4 nanoparticle composite for removal of ceftriaxone from aquatic solutions. J Mol
734 Liq 261:146–154. https://doi.org/10.1016/j.molliq.2018.04.019

735 Zhang Y, Geißen SU, Gal C (2008) Carbamazepine and diclofenac: Removal in wastewater
736 treatment plants and occurrence in water bodies. Chemosphere 73:1151–1161

737 Zimmermann SG, Wittenwiler M, Hollender J, et al (2011) Kinetic assessment and modeling of
738 an ozonation step for full-scale municipal wastewater treatment: Micropollutant

739 oxidation, by-product formation and disinfection. Water Res 45:605–617.
740 https://doi.org/10.1016/J.WATRES.2010.07.080

741

742

743

Tables

Table 1 – Mass ratios of PAC to iron salt mixture in the studied materials

PAC source	Nomenclature	PAC:Fe salt (*w/w*)	PAC % (*w/w*)
Waste-based	WPAC	(1:0)	100
	MAC2	(1:2)	33
	MAC3	(1:3)	25
	MAC4	(1:4)	20
	MAC6	(1:6)	14
Commercial	PBFG4	(1:0)	100
	MCAC2*	(1:2)	33
---	MP1	(0:1)	0

*Obtained from PBFG4 (commercial PAC provided by ChemViron)

Table 2 – Textural and magnetic properties of the adsorbents

Physical characterization	Adsorbents							
	WPAC	MAC2	MAC3	MAC4	MAC6	PBFG4*	MCAC2	MP1
S_{BET} ($m^2\ g^{-1}$)	1533	805	652	551	449	848	448	23
V_p ($cm^3\ g^{-1}$)	1.06	0.77	0.60	0.60	0.44	0.36	0.41	0.16
W_0 ($cm^3\ g^{-1}$)	0.61	0.32	0.26	0.22	0.18	0.30	0.18	0.01
D (nm)	1.39	1.32	1.85	2.17	1.97	0.84	1.81	13.59
M_S (emu g^{-1})	0.00	22.81	36.13	39.84	56.39	-	-	55.31

*Results provided from Calisto et al. (2014)

Table 3 – Fitting parameters of pseudo-first and pseudo-second order kinetic models and of Langmuir and Freundlich equilibrium models for the experimental data of the adsorption of CBZ in ultrapure and WWTP effluent for MAC4 and WPAC (Silva et al. 2019).

		Ultrapure water		WWTP effluent	
		MAC4	WPAC (Silva et al. 2019)	MAC4	WPAC (Silva et al. 2019)
Kinetic models					
Experimental q_e		87 ± 5	188 ± 4	61 ± 12	188 ± 7
Pseudo 1st order	q_e	87 ± 2	175 ± 7	60 ± 1	179 ± 4
	k_1	0.5 ± 0.1	0.038 ± 0.007	0.12 ± 0.01	0.09 ± 0.01
	R^2	0.986	0.940	0.984	0.989
	ASS	91.35	-	51.93	-
	$S_{y/x}$	3.902	16.60	2.942	7.59
Pseudo 2nd order	q_e	88 ± 2	192 ± 7	65 ± 2	188 ± 5
	k_2	0.03 ± 0.02	0.00027 ± 0.00005	0.003 ± 0.0005	0.0009 ± 0.0002
	R^2	0.987	0.974	0.985	0.990
	ASS	89.58	-	50.12	-
	$S_{y/x}$	3.864	10.81	2.890	7.22
Isotherm models					
Langmuir	q_m	68 ± 4	212 ± 16	60 ± 3	209 ± 27
	k_L	13 ± 12	2.8 ± 0.8	19 ± 21	0.6 ± 0.2
	R^2	0.968	0.965	0.995	0.984
	ASS	121.1	-	14.18	-
	$S_{y/x}$	4.493	13.73	1.684	8.12
Freundlich	k_F	63 ± 2	149 ± 8	56.6 ± 0.8	82 ± 10
	n	27 ± 37	4 ± 1	26 ± 32	2.3 ± 0.5
	R^2	0.963	0.928	0.995	0.975
	ASS	141.0	-	14.92	-
	$S_{y/x}$	4.847	19.84	1.728	10.03

q_e (mg g^{-1}); k_1 (min^{-1}); k_2 (g mg^{-1} min^{-1}); q_m (mg g^{-1}); K_L (L mg^{-1}); K_F ($mg^{1-1/n}$ $L^{1/n}$ g^{-1})

Table 4 – Comparison of adsorption capacities of selected examples of different adsorbents for CBZ removal

Adsorbent	Precursor	Matrix	Experimental conditions	Adsorption capacity (mg g^{-1})	Reference
Magnetic activated carbon	Coconut shells	Ultrapure water	pH = 6 T = 25 °C	135.1	(Shan et al. 2016)
Magnetic nanocomposite of activated carbon	Commercial activated carbon	Wastewater	pH = 6.65 T = 25 °C	182.9	(Baghdadi et al. 2016)
Graphene oxide composite	Functionalized with activated carbon and chitosan	Ultrapure water	T = 30 °C	11.2	(Delhiraja et al. 2019)
Phosphorised carbonaceous adsorbent	Lignocellulosic waste biomass	Ultrapure water	pH = 6 T = 22 °C	21.895	(Turk Sekulic et al. 2019)
Biopolymer electrospun nanofibers	Moringa seeds protein/PVA	Wastewater	pH = 5.5 T = 27 °C	31.25	(Kebede et al. 2019)
Magnetic powdered activated carbon (MAC4)	Primary paper mill sludge	Ultrapure water	T = 25 °C	68	This study
		Wastewater	pH = 8.07 T = 25 °C	60	

Figure captions

Scheme 1 – Schematic representation of the experimental approach followed for materials' production and adsorptive studies.

Figure 1 – Graphical representation of TOC and IC results for the cellulosic waste (PS), WPAC and produced MAC (PBFG4 results provided from [52]). Each bar corresponds to three replicates; standard deviations are too low to be perceptible.

Figure 2 – XRD patterns of WPAC, MP1 and MAC4.

Figure 3 – SEM images for MAC2, MAC3, MAC4 and MAC6 at magnifications of 10 000x and 50 000 x.

Figure 4 – CBZ removal percentage and associated standard deviation graphical representation of the preliminary adsorption studies at an adsorbent dosage of 25 mg L^{-1} and 50 mg L^{-1}.

Figure 5 – Graphical representation of the experimental data and pseudo-first and pseudo-second order model fittings for the kinetic adsorption studies using MAC4 in ultrapure water and WWTP effluent.

Figure 6 - Graphical representation of the experimental data and the isothermal model fittings (Langmuir and Freundlich) for the equilibrium adsorption studies using MAC4 in ultrapure water and WWTP effluent.

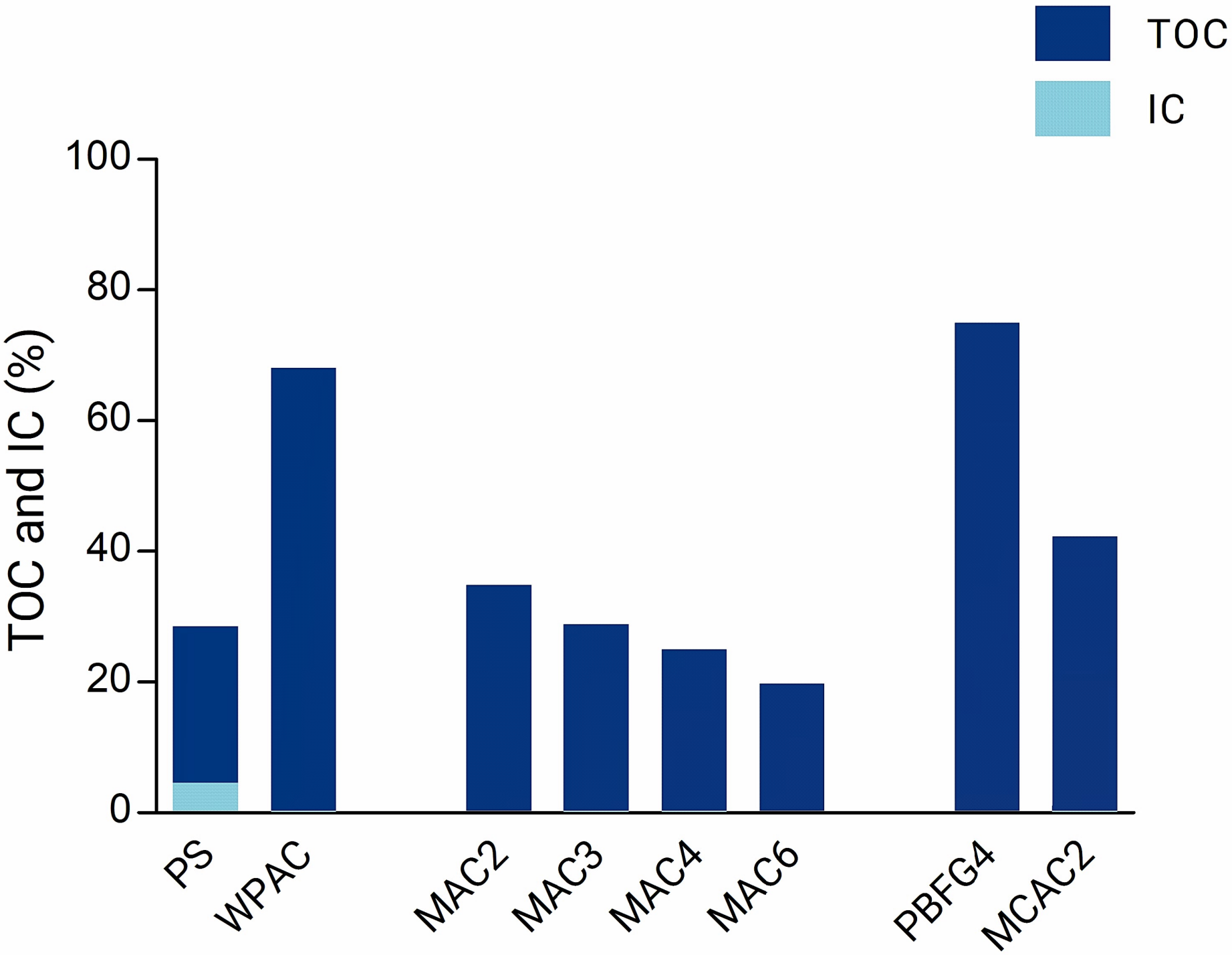
TOC
IC
TOC and IC (%)
100
80
60
40
20
0
PS
WPAC
MAC2
MAC3
MAC4
MAC6
PBFG4
MCAC2

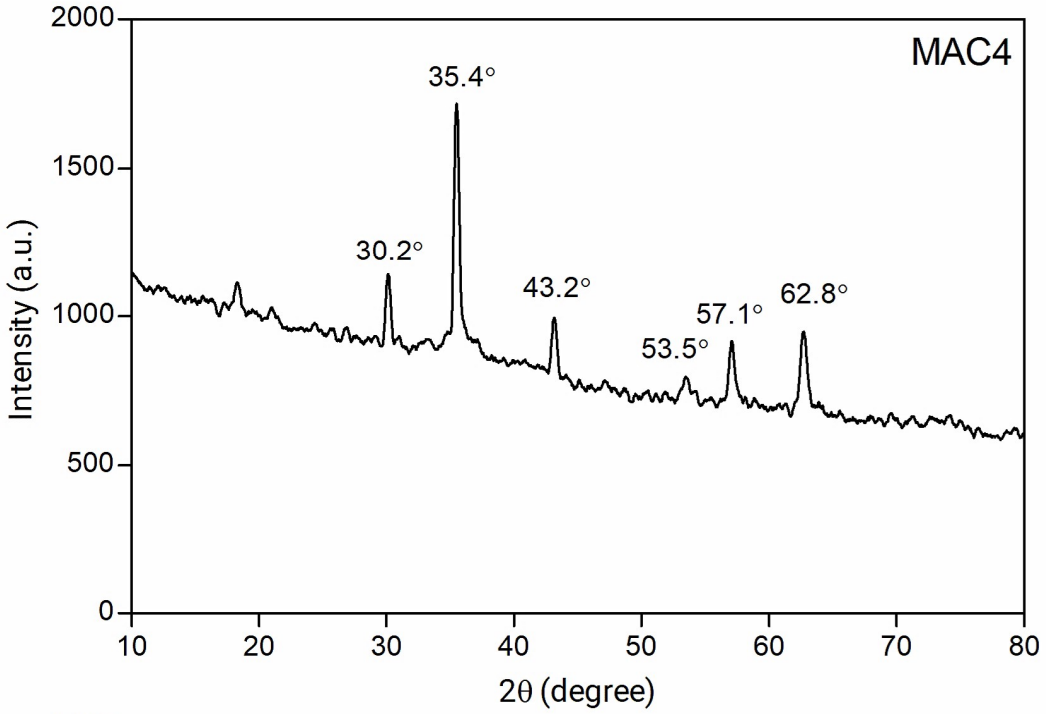
MAC4
35.4°
30.2°
43.2°
57.1°
62.8°
53.5°
Intensity (a.u.)
2θ (degree)

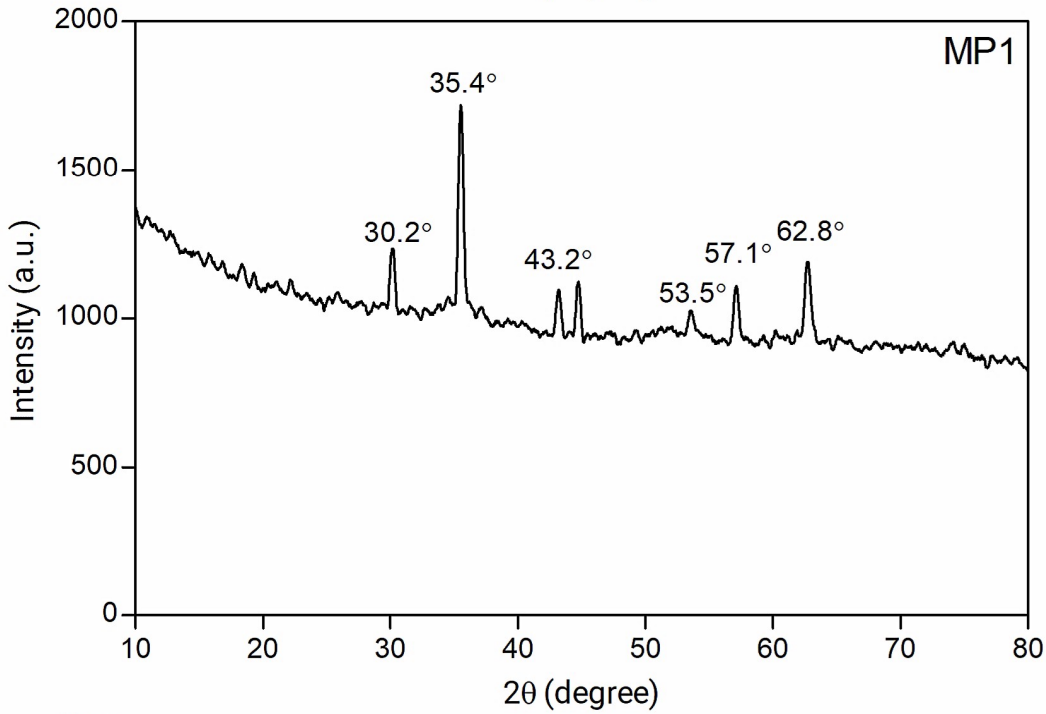
MP1
35.4°
30.2°
43.2°
57.1°
62.8°
53.5°
Intensity (a.u.)
2θ (degree)

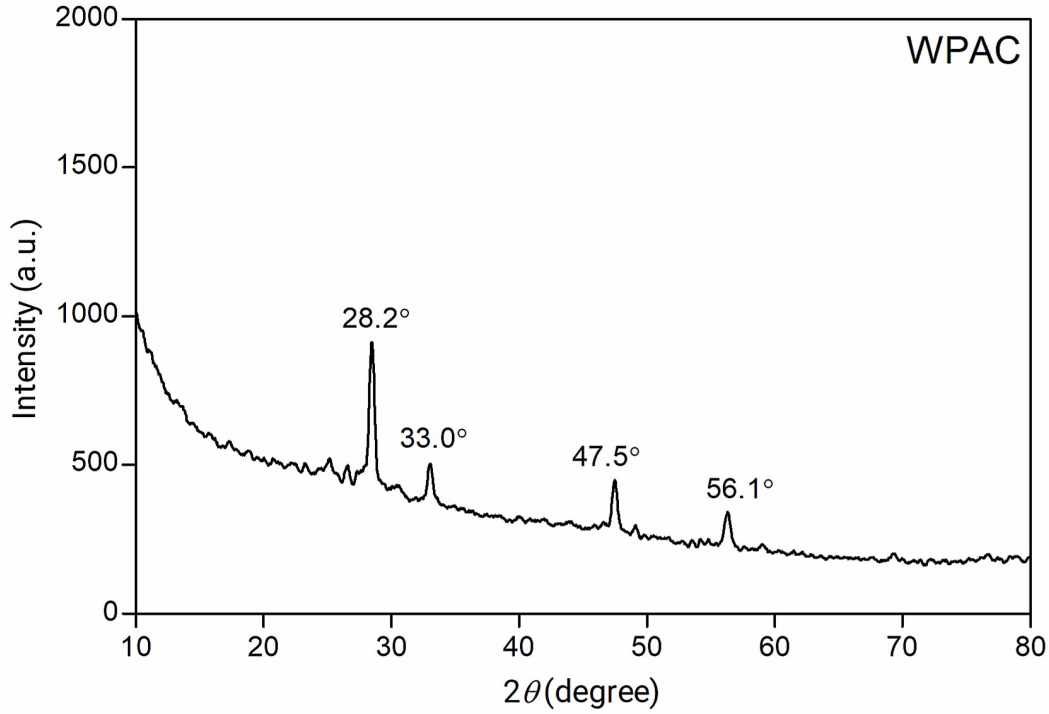
WPAC
28.2°
33.0°
47.5°
56.1°
Intensity (a.u.)
2θ (degree)

10 000 x

50 000 x

MAC2

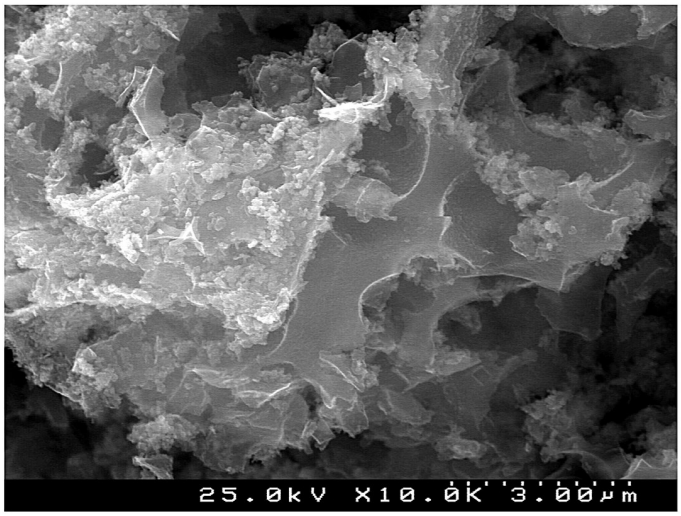

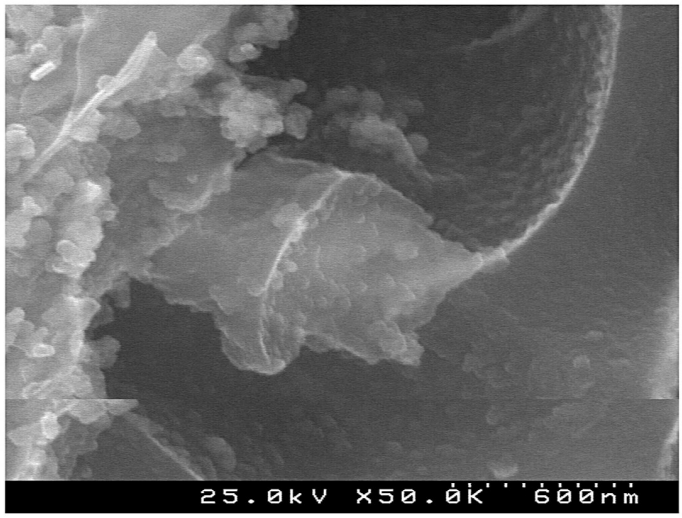

MAC3

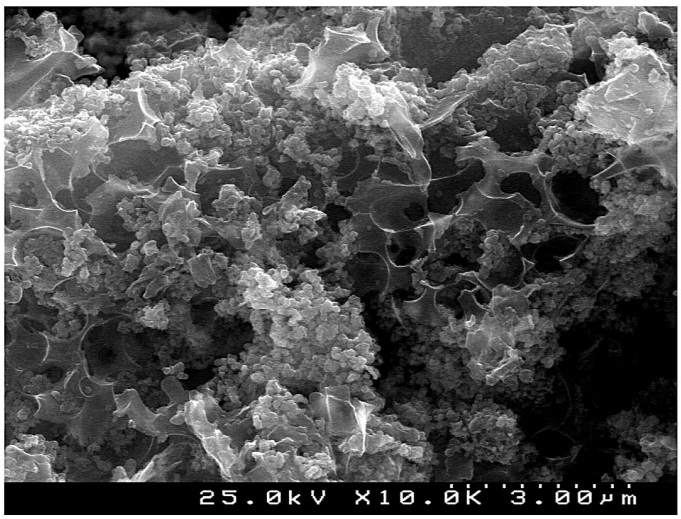

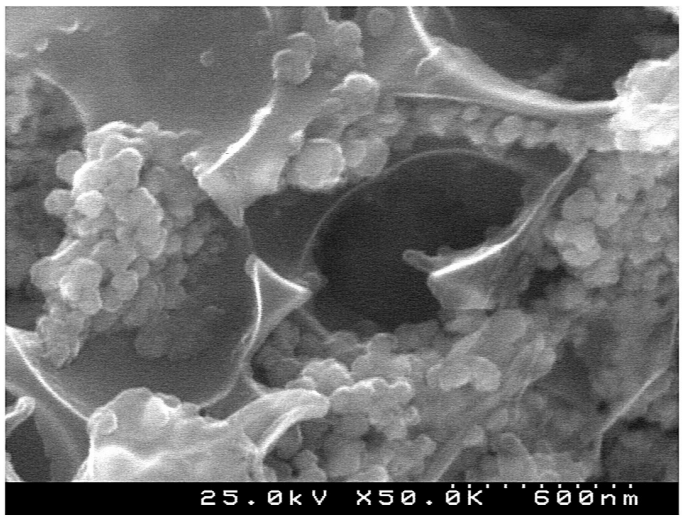

MAC4

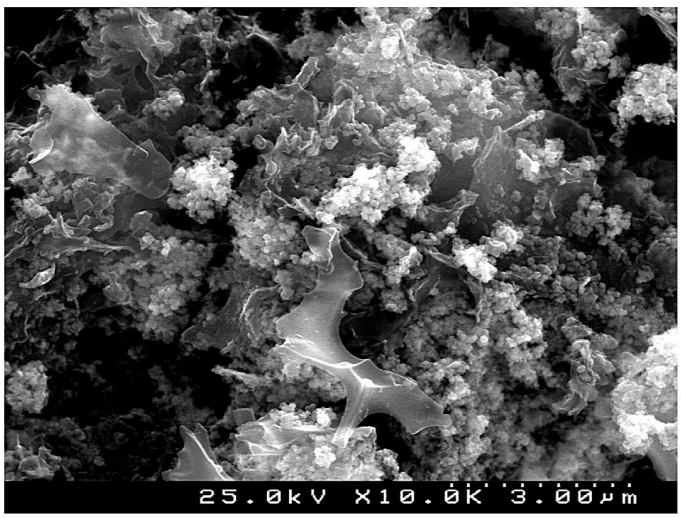

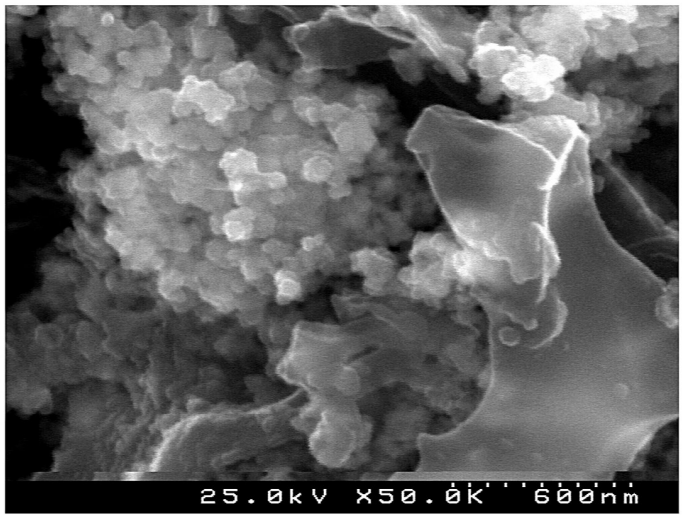

MAC6

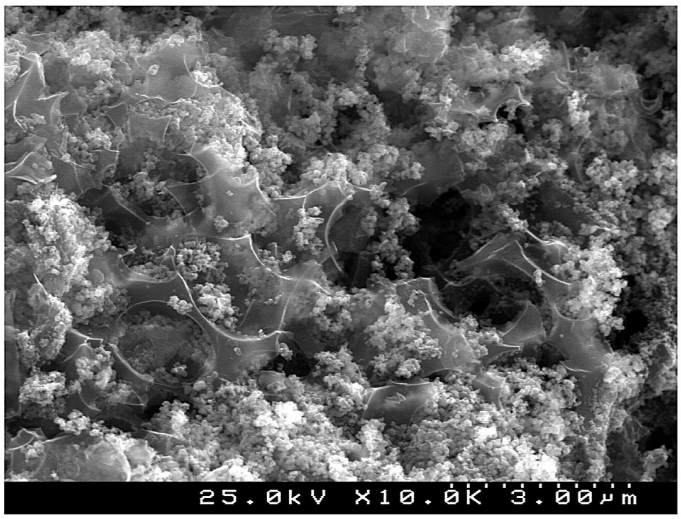

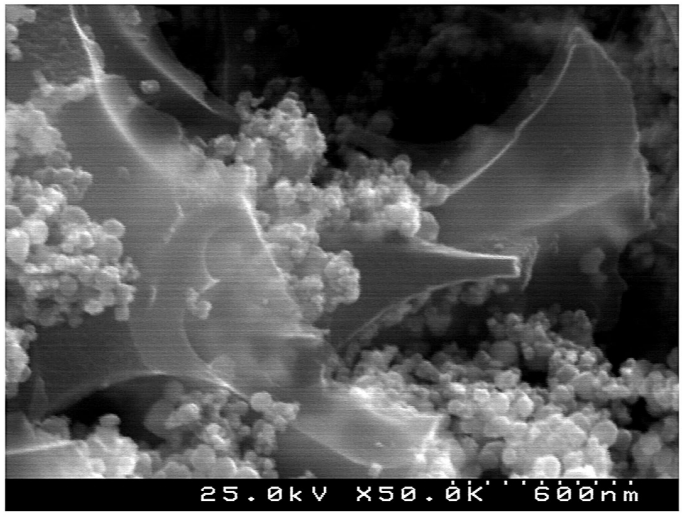

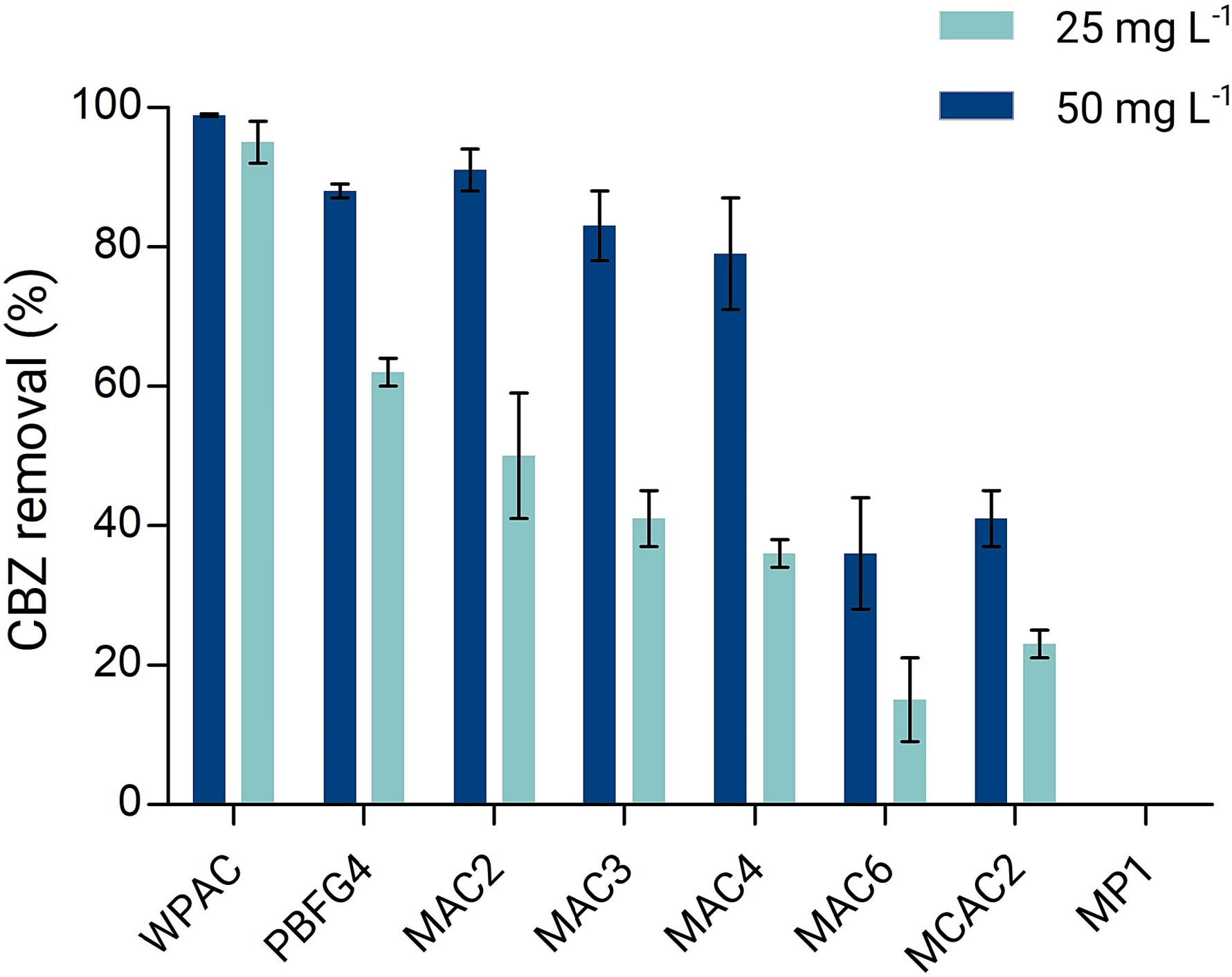
25 mg L-1
50 mg L-1
CBZ removal (%)
100
80
60
40
20
0
WPAC
PBFG4
MAC2
MAC3
MAC4
MAC6
MCAC2
MP1

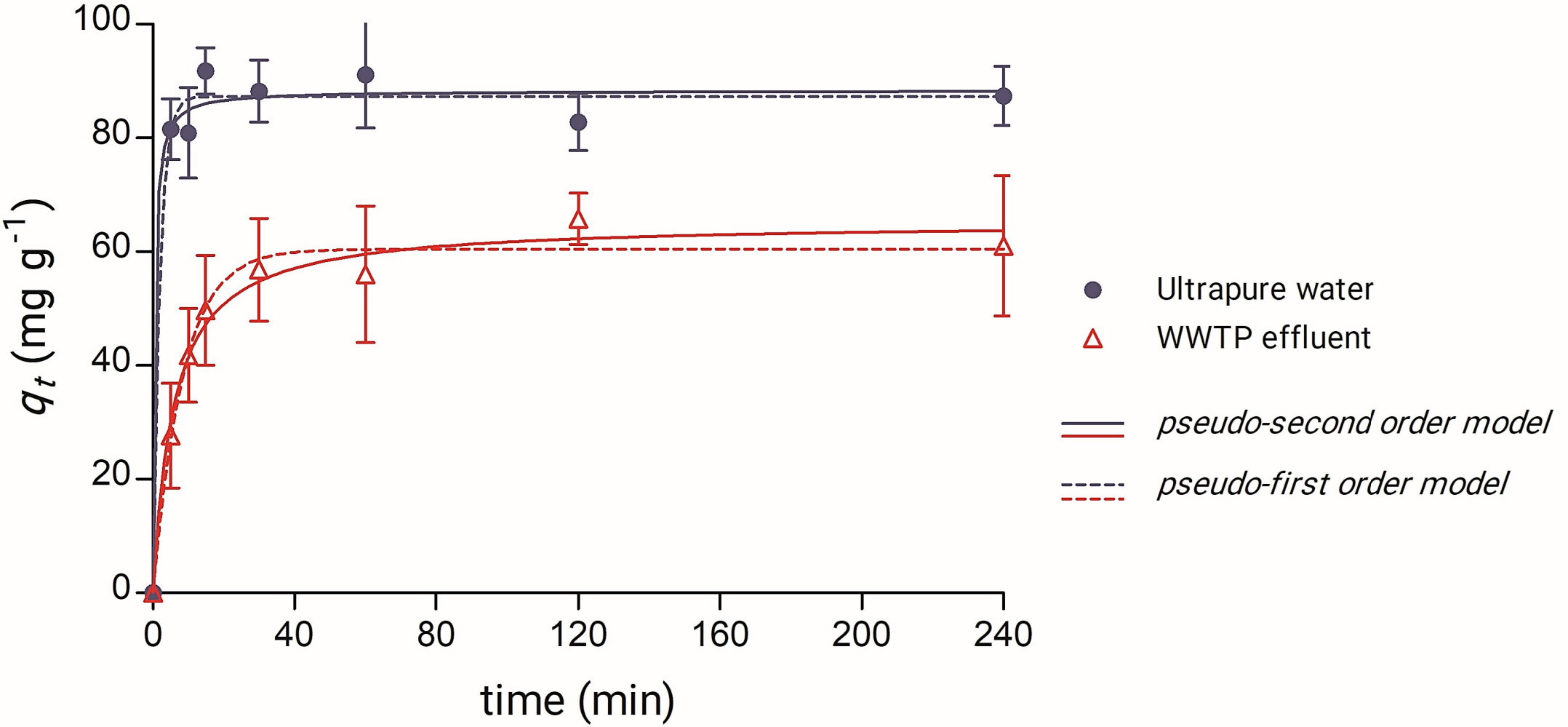
100
80
60
40
20
0
q_t (mg g^{-1})
0
40
80
120
160
200
240
time (min)
Ultrapure water
WWTP effluent
pseudo-second order model
pseudo-first order model

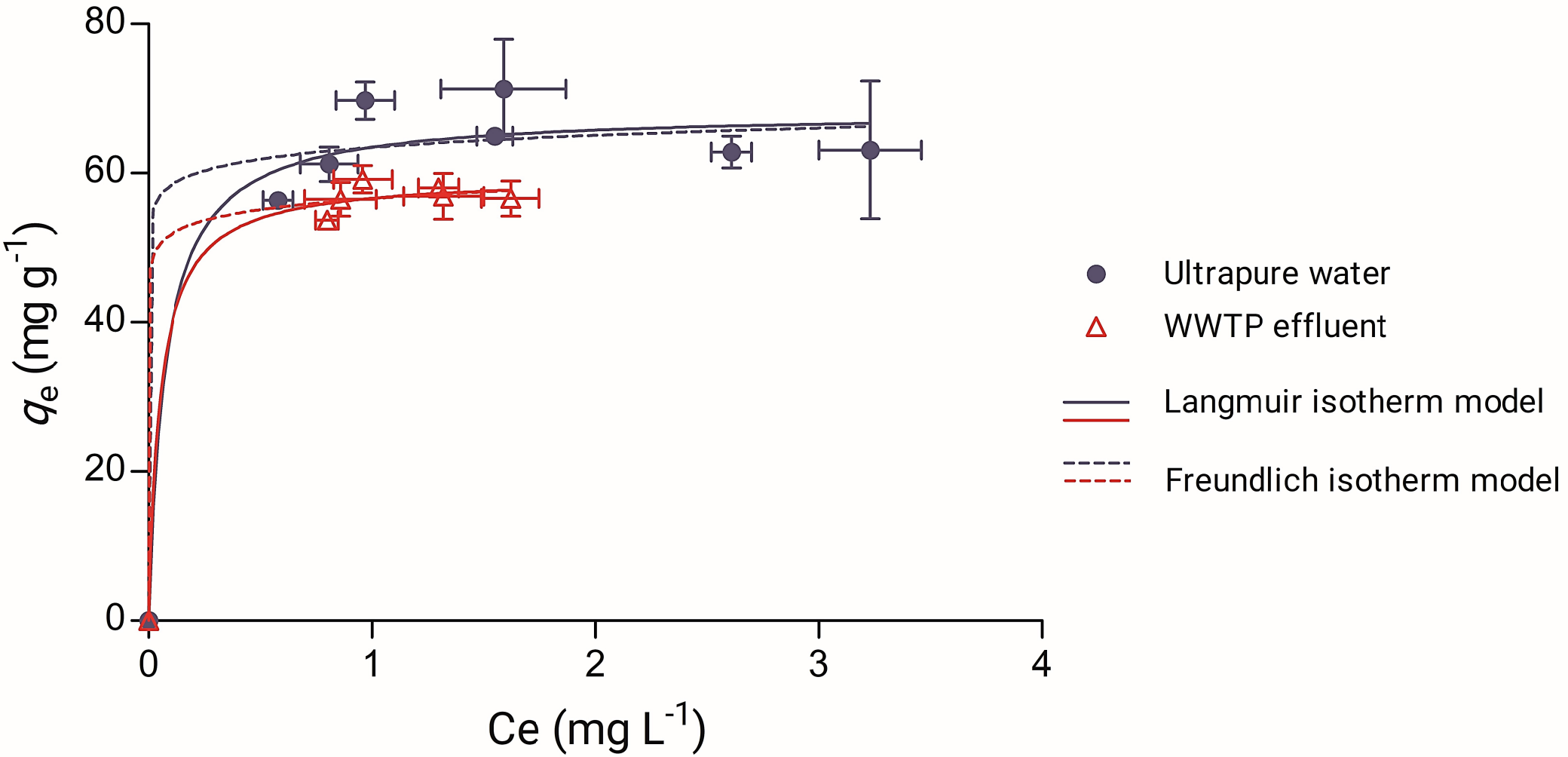
80
60
40
20
0
q_e (mg g^{-1})
0
1
2
3
4
Ce (mg L^{-1})
Ultrapure water
WWTP effluent
Langmuir isotherm model
Freundlich isotherm model